



Chemical updates
and radiative effects

K. M. Seltzer et al.

Evaluation of updated nitric acid chemistry on ozone precursors and radiative effects

K. M. Seltzer¹, W. Vizuete², and B. H. Henderson¹

¹Department of Environmental Engineering Sciences,
University of Florida, Gainesville, FL, USA

²Department of Environmental Science and Engineering,
University of North Carolina, Chapel Hill, NC, USA

Received: 18 December 2014 – Accepted: 6 January 2015 – Published: 3 February 2015

Correspondence to: B. H. Henderson (barronh@ufl.edu)

Published by Copernicus Publications on behalf of the European Geosciences Union.

Title Page

Abstract

Introduction

Conclusions

References

Tables

Figures



Back

Close

Full Screen / Esc

Printer-friendly Version

Interactive Discussion



Abstract

This study shows that revising the reaction rate of $\text{NO}_2 + \text{HO}^\bullet \rightarrow \text{HNO}_3$ improves simulated nitrogen partitioning and adjusts the simulated radiative effects of several radiative forcing variables. Both laboratory and field study analysis have found that the reaction rate should be reduced by 13–30 % from current recommendations. We evaluate the GEOS-Chem model over North America with and without the recommended update. Revising the $\text{NO}_2 + \text{HO}^\bullet \rightarrow \text{HNO}_3$ rate coefficient improves model performance by increasing NO_x concentrations in the upper troposphere and decreasing HNO_3 throughout the troposphere. The downward revision of the $\text{NO}_2 + \text{HO}^\bullet \rightarrow \text{HNO}_3$ rate increases the lifetime of NO_x , increases O_3 concentrations and increases the simulated radiative effects of tropospheric ozone. These findings demonstrate the influence the rate revision has on the composition of the atmosphere, the benefits it provides when compared to observations and the simulated radiative effects that the reduction induces.

1 Introduction

Global chemical transport models (GCTMs) are excellent tools for exploring our scientific understanding. They are used to estimate concentrations fields, develop source/sink budgets for compounds, source/receptor relationships, infer emission inventories, and estimate impact of emission reduction strategies (e.g., Jaeglé et al., 2003; Fusco and Logan, 2003; West et al., 2006; Chen et al., 2009; Millet et al., 2010; West et al., 2009; Kopacz et al., 2010). The benefit of GCTMs to their regional counterparts is the scale that decreases sensitivity to boundary conditions. The trade off is increased sensitivity to modeled processes including emissions, transport, and chemistry. The uncertainty in processes can have competing effects that make them difficult to identify even when the uncertainty influences the research subject. When new information on a process emerges in the literature, the GCTM must be evaluated in the

Title Page

Abstract

Introduction

Conclusions

References

Tables

Figures



Back

Close

Full Screen / Esc

Printer-friendly Version

Interactive Discussion



context of that new information. We must also understand how updating a process would have influenced conclusions from previous studies.

GCTMs are often used to predict or estimate the ozone and aerosols that are products of photochemical oxidation. In the context of oxidation, the chemical component of GCTMs (a.k.a. chemical mechanism) indirectly influences all the other processes. Chemical transformation directly changes the chemical availability of compounds and the physical properties of compound families. For instance, reaction R1 decreases the photochemical availability of a hydroxyl radical (HO^\bullet) and nitrogen oxides ($\text{NO}_x = \text{NO} + \text{NO}_2$). Reaction R1 also increases the solubility of oxidized nitrogen because the Henry's Law coefficient for HNO_3 ($2.1 \times 10^5 \text{ Matm}^{-1}$ at 298 K) is seven orders of magnitude greater than that of NO_2 ($10^{-2} \text{ Matm}^{-1}$ at 298 K). Uncertainty in reaction R1 would, therefore, affect the lifetime of NO_x emissions and the lifetime of NO_y as a NO_x reservoir. This is particularly important to ozone in its climate forcing capacity because, on average, ozone production is limited by NO_x availability (Sillman et al., 1990; McKeen et al., 1991; Chameides et al., 1992; Jacob et al., 1993; Jaeglé et al., 1998).



Reaction R1 is widely recognized as a key reaction in atmospheric oxidation (e.g., Seinfeld, 1989; Donahue, 2011), but has not been well constrained. Despite its known influence, reaction R1 has proved difficult to measure at temperatures and pressures in the troposphere (Donahue, 2011). In a recent study, Mollner et al. (2010) employed state-of-the-science techniques to accurately measure the rate at standard temperature and pressure ($T = 298 \text{ K}$ and $P = 1 \text{ atm}$). In a subsequent study, Henderson et al. (2012) constrain the rate of reaction R1 using aircraft measurements from the upper troposphere ($T = 240 \text{ K}$ and $P = 0.29 \text{ atm}$). Both of the studies above recommend significant downward revisions of the rate, and the rate recommended in the upper troposphere suggests an update to the temperature sensitivity (Henderson et al., 2012).

Chemical updates and radiative effects

K. M. Seltzer et al.

Title Page

Abstract

Introduction

Conclusions

References

Tables

Figures

◀

▶

◀

▶

Back

Close

Full Screen / Esc

Printer-friendly Version

Interactive Discussion



**Chemical updates
and radiative effects**

K. M. Seltzer et al.

Title Page

Abstract

Introduction

Conclusions

References

Tables

Figures



Back

Close

Full Screen / Esc

Printer-friendly Version

Interactive Discussion



Updates to the rate of reaction R1 have the potential to change NO_x concentrations, radical concentrations, ozone concentrations and sensitivity to emission reduction strategies (Cohan et al., 2010). As well, since tropospheric ozone has strong influences on the radiative budget of the atmosphere, changes in the atmospheric radiation balance predicted by GCTMs will occur. This study implements the updated rates in the GEOS-Chem chemical transport model and evaluates the impact. In addition to the effects on ozone precursors, the study also utilizes an offline radiative transfer model to evaluate the predicted direct radiative forcing (DRF) changes that this mechanism update produces. We hypothesize that increased NO_x lifetime will increase NO_x concentrations, decrease HNO_3 concentrations, reduce the ratio of HO_2^* to HO^* concentrations, increase ozone sensitivity to NO_x emission reductions, and lead to localized positive radiative effects in locations where ozone increases occur.

2 Methods

In this study, we evaluate the influence the updated chemical mechanism has on model estimates of trace gas composition in the troposphere and radiative effects on the surface and effective top of atmosphere. The base model will be described in Sect. 2.1 and the chemistry updates in the Sect. 2.2. The observations and their associated uncertainty are described in the Sect. 2.3. The method of evaluation used to incorporate measurement uncertainty is described in the Sect. 2.4. The methods used to determine the radiative effects of the chemical mechanism update are discussed in the Sect. 2.5 section.

2.1 Model description

We simulate the INTEX-A time period (July–August 2004) using the GEOS-Chem global chemical transport model (version 9-01-02; <http://www.as.harvard.edu/chemistry/trop/geos/>). The GEOS-Chem model explicitly simulates tracer species ad-

**Chemical updates
and radiative effects**

K. M. Seltzer et al.

Title Page

Abstract

Introduction

Conclusions

References

Tables

Figures



Back

Close

Full Screen / Esc

Printer-friendly Version

Interactive Discussion



vection, diffusion, deposition, gas-phase reactions, equilibrium partitioning of gas to aerosol using inputs for meteorology, emissions, and chemistry inputs to produce predictions concentration fields. We configured GEOS-Chem to produce concentration fields from 1 July to 30 August. The concentration fields are produced at 2° by 2.5° and 47 vertical levels. We evaluated levels 1 through 32, which range in resolution from 120 m near the surface to 1000 m at the top. The simulated time frame covers the period observed by the National Aeronautics and Space Administration (NASA) aircraft (DC-8). Although we have simulated global fields, the model evaluation will cover the Northern Hemisphere, primarily over North America (see Fig. 1). The meteorological inputs are produced by the NASA Global Modeling and Assimilation Office (GMAO) and assimilate observations from the Goddard Earth Observing System version 5 (GEOS-5). The GEOS-5 system is the latest version and has observations starting on 1 January of 2004. The model was configured to use cloud convection with a 15 min timestep and planetary boundary mixing with the non-local option. The emissions include biomass (van der Werf et al., 2006), biogenic (Guenther et al., 2006), lightning (Ott et al., 2010), and anthropogenic emissions (described below).

Anthropogenic emissions of NO_x , CO , and SO_2 are included at both a global and regional scale. At the regional scale, anthropogenic emissions of NO_x , CO , and SO_2 are specifically provided for the United States of America, Europe, Mexico and South-East Asia. The United States emissions are derived from the EPA's National Emission Inventory (NEI) for the year 2005 and supplemented by the biofuel emission inventory from 1999. In contrast to the 1999 NEI, the mobile NO_x emissions from the 2000 NEI have compared well to fuel use estimates (Parrish, 2006; Dallmann and Harley, 2010). The European emissions are provided by the Co-operative Programme for Monitoring and Evaluation of the Long-range Transmission of Air Pollutants in Europe (EMEP) inventory for Europe in 2000 by Vestreng and Klein (2002). The Mexico emissions are derived from the 1999 Big Bend Regional Aerosol and Visibility Observational (BRAVO) emissions inventory for Mexico (Kuhns et al., 2003). The Asia emissions are derived

from Streets et al. (2003, 2006). For the rest of the world, emissions are included from the EDGAR fossil fuel inventory and scaled from the year 2000 (Olivier et al., 2002).

2.2 Chemistry updates

In this study, we compare simulations with standard chemistry (base case) and revised chemistry (HNO₃ case). The reaction rate of NO₂ + HO[•] is decreased to account for emerging literature recommending a downward revision (Mollner et al., 2010; Henderson et al., 2012). The recommendation by Mollner et al. (2010) is 13 % below the rate recommended by Sander et al. (2011), which is lower than that recommended by Atkinson et al. (2004). Donahue (2011) commended the recent work by Mollner et al. (2010), but asserted that there is remaining uncertainty. Henderson et al. (2012) also re-evaluated the rate constant using Bayesian inference and measurements from the upper troposphere. The evaluation in the upper troposphere complements the Mollner et al. (2010) study with information at temperatures from 230–250 K. Henderson et al. (2012) conclude that the temperature sensitivity is currently overestimated and should be revised according to Eqs. (1) and (2).

$$k_0 = 1.49 \times 10^{-30} \left(\frac{T}{300} \right)^{-1.9} \quad (1)$$

$$k_\infty = 2.58 \times 10^{-11} \quad (2)$$

2.3 Observations

In this study, we evaluate the model with respect to aircraft observations from the INTEX-A campaign. The INTEX-A campaign collected observations from 90 m to 11.9 km covering North America. The suite of measurements includes inorganic species NO, NO₂, PAN, HNO₄, HNO₃, O₃, H₂O₂ and CO and organic species CH₂O, CH₃CHO, and CH₃C(O)CH₃. As with other studies (e.g., Hudman et al., 2007), the observations are filtered to exclude stratospheric intrusion, biomass burning, wildfires, and fresh pollution plumes. These events are excluded because the model is

Chemical updates and radiative effects

K. M. Seltzer et al.

Title Page

Abstract

Introduction

Conclusions

References

Tables

Figures



Back

Close

Full Screen / Esc

Printer-friendly Version

Interactive Discussion



Chemical updates
and radiative effects

K. M. Seltzer et al.

Title Page

Abstract

Introduction

Conclusions

References

Tables

Figures



Back

Close

Full Screen / Esc

Printer-friendly Version

Interactive Discussion



not designed to capture the variability of extreme events. First, plumes that are identified in the flight logs were removed. Then biomass burning is identified by hydrogen cyanide greater than 500 ppt or acetonitrile greater than 225 ppt. Fresh pollution plumes are identified where NO_x was more than 40 % of total oxidized nitrogen ($\text{NO}_y \equiv \text{NO}_x + \text{PAN} + \text{HNO}_3$), or if NO_y is not available, when $\text{NO}_2 > 400$ ppt and below 3 km. Stratospheric intrusion is identified when the ratio of O_3 to CO is greater than 1.25.

For each measurement, an estimation or calculation of the uncertainty of the measurement technique was carried out. Depending on the measurement, the uncertainty was either provided for the whole dataset or on a per-sample basis. Absolute uncertainty is provided on a per sample basis, while relative uncertainty is provided for the dataset. Relative uncertainty (1σ) was provided for O_3 ($\pm 5\%$), HO^* ($\pm 15\%$), HO_2^* ($\pm 15\%$), PAN ($\pm 15\%$), and NO_2 ($\pm 5\%$). For HNO_3 (measured by P. Wennberg at the California Institute of Technology), uncertainty was provided as a column-wise absolute uncertainty that combines calibration, water correction, and background signal. The uncertainty was propagated from the 0.5 s time-scale to the 1 min time-scale through linear propagation ($\sigma = \sqrt{n^{-1} \sum_i^n \sigma_i^2}$). The HNO_3 relative error simple average is 20 %, median is 12 %, 75th percentile is 19 %, and the concentration weighed average is 11 %.

For the NO_2 measurement, the measurement has a known interference at low temperatures (Browne et al., 2011). At low ambient temperatures, pernitric acid (HNO_4) and methyl peroxy nitrate ($\text{CH}_3\text{O}_2\text{NO}_2$) dissociate in the inlet tube, adding molecules of NO_2 to the measurement. When temperatures are above 255 K, the interference is less than 5 % and within stated uncertainty limits (Browne et al., 2011). When temperatures are below 255 K, the interference can be more than 15 %. Below 255 K, we use a chemical box-model (Henderson et al., 2012) to estimate the concentration of $\text{CH}_3\text{O}_2\text{NO}_2$ and reduce the NO_2 measurement accordingly. Post-analysis of $\text{CH}_3\text{O}_2\text{NO}_2$ suggests that this approach provided $\text{CH}_3\text{O}_2\text{NO}_2$ concentrations within a factor of two. Box-model median $\text{CH}_3\text{O}_2\text{NO}_2$ concentrations predicted 14 ppt at 8 km

and 17 ppt at 10 km. The GEOS-Chem model CH₃O₂NO₂ predictions are between 15 ppt from 8 to 9 km and 34 ppt from 9 to 10 km. Above 10 km, the uncertainty in our box model CH₃O₂NO₂ predictions increase, which leads us to evaluate only below 10 km. Although there are differences, they are insufficient in magnitude to alter our conclusions.

For nitric oxide (NO), the direct measurement is not sensitive at concentrations studied here. Nitric oxide (NO) was measured by chemiluminescence with a 50 ppt lower-limit of detection, which is too high to characterize the middle free troposphere (e.g., Bertram et al., 2007; Singh et al., 2007). As a result, we calculate steady-state NO as described in Eq. (3), where j is the photolysis rate, T is temperature, and “[]” denote concentrations. The uncertainty in the derived NO value is propagated from NO₂, O₃, and HO₂ with the assumption that temperatures and reaction rates are precisely known.

$$[\text{NO}]_{\text{ss}} = \frac{j[\text{NO}_2]}{3.3 \times 10^{-12} \times \exp\left(\frac{270}{T}\right) [\text{HO}_2] + 3.0 \times 10^{-12} \times \exp\left(\frac{-1500}{T}\right) [\text{O}_3]} \quad (3)$$

In addition to individual measurements, this analysis focuses on species groups and algebraic combinations of measurements. The two most notable species groups are NO_x (NO + NO₂) and NO_y (NO_x + PAN + HNO₃). The uncertainty for species groups is simply the root of the summed squared error.

Descriptive statistics and uncertainties for INTEX-A measurements are characterized in Table 1. The table summarizes uncertainty evaluated for the whole dataset, but uncertainty at each altitude varies. For each measurement, Table 1 shows the number of valid measurements, mean (\bar{X}), percentiles (5, 50, and 75 %), and mean uncertainties (relative $\left(\frac{\sigma_x}{\bar{X}}\right)\%$; absolute $\bar{\sigma}_x$ in measurement units).

Chemical updates
and radiative effects

K. M. Seltzer et al.

Title Page

Abstract

Introduction

Conclusions

References

Tables

Figures



Back

Close

Full Screen / Esc

Printer-friendly Version

Interactive Discussion



2.4 Method of model evaluation

The simulations described above have inherent uncertainty and must be evaluated using observations that also have uncertainty. The simulations spatially average concentration over a 48 000 km² area, which can reduce the variance of chemical species by averaging highs and lows. The observations also spatially average, but only over line segments that range from 4 to 17 km. Based on these differences alone, we expect the observed and simulated set will each have its own mean and variance for each chemical species. The mean concentration for a log-normally distributed species (e.g., NO_x, HNO₃) is highly sensitive to the variance of the results. For log-normally distributed species, the means cannot be compared because the variances are expected to be different. In this case, the species can be log-transformed to reduce the bias of the mean, but the variances of the observations and model are still different. The difference in variances precludes certain statistical evaluation techniques.

We account for different variances and observational uncertainty using a variant of the Student's *t* test. The Student's *t* test assumes that the variances of the two populations are identical. The variances are not expected to be identical and, therefore, the standard Student's *t* test is not appropriate for this evaluation. The Welch's *t* test (hereafter *t* test) is a variant of the Student's *t* test that calculates the combined variance using the Welch–Satterthwaite equation (Welch, 1947). Although the *t* test can now compare the measurements and predictions, it cannot yet account for measurement accuracy. The *t* test estimates the probability that the measured and modeled mean could be obtained given repeated sampling with the assumption that the true means are the same. This type of test does not inherently account for potential bias in the measurements, but can be used as part of a framework that does.

Having accounted for the variances, we must now address the reported accuracy and precision tolerances of the observations. The true bias of a measurement cannot be known until compared to a superior method under similar circumstances. There is, currently, insufficient data to fully characterize all the biases of measurements made

Title Page

Abstract

Introduction

Conclusions

References

Tables

Figures



Back

Close

Full Screen / Esc

Printer-friendly Version

Interactive Discussion



Chemical updates
and radiative effects

K. M. Seltzer et al.

Title Page

Abstract

Introduction

Conclusions

References

Tables

Figures

◀

▶

◀

▶

Back

Close

Full Screen / Esc

Printer-friendly Version

Interactive Discussion



during INTEX-A. For some measurements, however, multiple techniques produce different answers or subsequent analysis demonstrates a bias. For example, we now know that the NO_2 measurement has an interference from peroxy nitrates. The methyl peroxy nitrate interference ranges from 2.5 % at 265 K to 60 % at 225 K. Therefore, we need to estimate measurement accuracy and account for it in our evaluation technique.

In order to account for measurement uncertainty, we use a method referred to as two one-sided t tests (TOST) (Schuirmann, 1987). Using TOST, we can test whether the model predictions are within measurement uncertainty by rejecting one of two null hypotheses. The first null hypothesis is that the simulated mean is greater than the observations adjusted to their lower bound. The second null hypothesis is that the simulated mean is less than the observations adjusted to their upper bound. If we reject either hypothesis, we have rejected that the model is equivalent to the observations. This approach is equivalent to assuming a systematic bias equal to the uncertainty in the measurement.

Using relative uncertainty, we formulate the null hypotheses ($H_{0,1}$ and $H_{0,2}$) using products. For each measurement, the observed accuracy is based on an estimate, which can be found in the header of the observation files. An alternative formulation is to produce a confidence interval for the difference and compare that to the uncertainty of the mean. We did not use this approach because it does not account for adjustments to observational variance when uncertainty is provided as a factor.

$$H_{0,1} : \mu_{\text{mod}} \geq \mu_{\text{obs} \times (1-U)}$$

$$H_{a,2} : \mu_{\text{mod}} < \mu_{\text{obs} \times (1-U)}$$

$$H_{0,2} : \mu_{\text{mod}} \leq \mu_{\text{obs} \times (1+U)}$$

$$H_{a,2} : \mu_{\text{mod}} > \mu_{\text{obs} \times (1+U)}$$

The null hypotheses are formulated to give the benefit of doubt to the model. The joint null hypothesis is that the model is within uncertainty, which must be rejected to conclude that the model is different (greater or less than) from observations. A higher

bar would be equivalence testing where we reverse the null and alternative hypotheses. As defined, the analysis is conservative with respect to model evaluation.

For each simulation, we evaluate the model in 1 km vertical divisions to capture the influence of temperature, pressure, and transport. Temperature and pressure affect the rate of chemical reactions including the reactions that produce HNO₃. The affect of temperature/pressure sensitivity can, therefore, only be seen by evaluating the model with respect to altitude.

When using statistical tests like the *t* test, we must be careful to maintain the independent and identically distributed assumption. By default, the plane flight sampling in GEOS-Chem outputs one prediction for each observation. These pairs help to preserve identical distribution because observations and predictions will represent the same geographic regions. The model's larger spatial and temporal averaging, however, means that a model grid cell can be paired with more than one observation. In this case, the set of model predictions will contain duplicates that must be removed to maintain independence. After removing duplicates, we have two datasets (observations and predictions) that are each a representative sample of the atmosphere.

For each altitude, we compare the observed and simulated values of chemical concentrations. To reduce the influence of spatial averaging on variance, variables that demonstrate log-normal distributions will be log-transformed. By log transforming, the distribution becomes symmetric and reduces the skews influence on the mean. By converting all variables to normal distributions, we also allow for the use of statistical tests like the *t* test.

When equivalence of observations and simulations is rejected, we examine the bias further. For bias calculations, the duplicate model results are not removed. By retaining duplications, each observation can be paired with a prediction. This allows us to calculate the mean normalized bias (\bar{B}_N) as defined in Eq. (4). In Eq. (4), o_i is an ob-

**Chemical updates
and radiative effects**

K. M. Seltzer et al.

Title Page

Abstract

Introduction

Conclusions

References

Tables

Figures



Back

Close

Full Screen / Esc

Printer-friendly Version

Interactive Discussion



ervation, y_j is a prediction, and n is the number of pairs. The number of pairs varies by compound because some observations are more available than others.

$$\bar{B}_N = \frac{\sum_{i=1}^n \frac{y_i - o_i}{o_i}}{n} \quad (4)$$

We evaluate the model by using the t test for species and species groups and examining their bias. This evaluation will include the NO_x cycling that drives photochemical ozone production. For NO_x , it is important to evaluate the family of compounds involved in its cycling. As such, we evaluate NO_x and its products by defining NO_y as the sum of NO_x , PAN, and HNO_3 ($\frac{\text{NO}_x + \text{PAN} + \text{HNO}_3}{\text{NO}_x + \text{PAN} + \text{HNO}_3 + \text{HNO}_4 + \text{RNO}_3} > 88\%$ for 90% of all samples). Because there is a bias in NO_y (see Results), we also evaluate its components as a fraction of the total.

2.5 Radiative effects

Changes in nitric acid formation affect the concentrations of various short-lived climate forcers in the atmosphere. These changes result in variances in the radiative budget of the atmosphere and will change the predicted forcing at the surface and top of the model domain. For the updates to the nitric acid mechanism, these changes are largely driven by the changes in tropospheric ozone concentrations, which is a large contributor to the radiation balance of our atmosphere. To a lesser extent, changes in radiative effects due to the updated nitric acid mechanism include concentration differences of certain aerosols, such as sulfuric acid. Ultimately, as previously mentioned, a decrease in the reaction rate of nitric acid formation will increase tropospheric photochemical ozone production, which is largely limited by NO_x availability. This would have a positive increase in radiative effects in the atmosphere and the intensity of such radiative changes will largely be spatially and temporally heterogeneous. In addition, the nitric acid mechanism update can change the oxidation potential of the atmosphere. This

Chemical updates and radiative effects

K. M. Seltzer et al.

Title Page

Abstract

Introduction

Conclusions

References

Tables

Figures



Back

Close

Full Screen / Esc

Printer-friendly Version

Interactive Discussion



change can affect the formation of aerosols and has a potential to vary the concentration and distribution of aerosols, such as sulfuric acid. This process has the potential of creating negative radiative effects.

To assess the radiative effects of changing the nitric acid reaction rate, the Parallel Offline Radiative Transfer (PORT) model was utilized (Conley et al., 2013). This standalone model was developed at the National Center for Atmospheric Research (NCAR) and isolates the radiation code from the Community Atmosphere Model (CAM). By using this model, the direct radiative forcing due to the mechanism update can be quantified. Input to PORT was compiled using output from the GEOS-Chem simulations. An instantaneous tracer timeseries output was created every 73rd time step, which resulted in an output generated every 2190 min. This output schedule enabled a balance of sampling all seasons, day and night occurrences, output files sizes and overall computational strain. Conley et al. (2013) found such a sub-sampling routine to have less than a 0.1 % relative error in the radiative flux when compared to a PORT simulation using every time sample. Radiative effects due to ozone, sulfate, organic and black hydrophilic and hydrophobic carbon, sea salt and dust were quantified using PORT. While the main drivers of the radiative effects due to the mechanism update will be driven by ozone, and to a lesser extent sulfate aerosols, all of these variables were included due to availability.

3 Results

3.1 Aircraft evaluation

In this section, the base case and HNO₃ case models are compared to the INTEX-A observations, with a focus on ozone, nitrogen, and nitrogen partitioning. Each component is evaluated in 1 km bins from the surface (0 km) to 10 km. Initial evaluation of total oxidized nitrogen (NO_y = NO_x + PAN + HNO₃) shows a high bias associated with NO_x

Chemical updates and radiative effects

K. M. Seltzer et al.

Title Page

Abstract

Introduction

Conclusions

References

Tables

Figures



Back

Close

Full Screen / Esc

Printer-friendly Version

Interactive Discussion



production from lightning. Fig. 2 displays the vertical emission profile of lightning in the model and a general overprediction of NO_x can be seen in Fig. 3a.

Since a high bias exists for NO_y throughout much of the atmosphere, the remaining evaluation of ozone, nitrogen and nitrogen partitioning from the updated mechanism will feature a NO_y normalization. Figure 3 shows total oxidized nitrogen (NO_y) and its components (NO_x , PAN, and HNO_3). Each of the components are shown as a normalized percentage of NO_y . For each 1 km bin, Fig. 3 shows the mean (black dots) and 90 % range (5–95 %) of the observed (grey bars) and simulated values (base: blue, HNO_3 : red). The dots that represent the simulated means are black if the model is consistent with the observations (i.e., we cannot reject $H_{0,1}$ and $H_{0,2}$). Figure 3a shows that NO_y performance changes as a functional of altitude. In the upper troposphere (8–10 km), all the models are consistent with observations. Simulated NO_y , however, is less concave than observed and all the models are high-biased from 0 to 8 km, where observed values are at their minimum.

The target of improved chemistry is above 8 km, so the biases below 7 km will be addressed separately. Between 8 and 10 km, the updated chemistry improves the predictions of NO_x , HNO_3 , and PAN. For NO_x , both cases are low-biased from 8 to 10 km; however, the HNO_3 case shows significant improvements. For HNO_3 , both the base and HNO_3 cases are high-biased from 8 to 10 km, but once again, the HNO_3 case shows significant improvements. This is especially seen in the 8 to 9 km bin, where observed and simulated values no longer show statistical differences. For HNO_3 , Fig. 3c shows that the two cases are statistically consistent with observations from 0 to 10 km, with an exception of the base case in this 8 to 9 km bin. On an overall basis, the HNO_3 case improves model performance and is consistent with observations at all levels. For PAN, the HNO_3 case improves predictions at all levels above 3 km, though there are many bins of statistically significant low bias between 4 and 9 km. However, this is seen in both simulated scenarios and is improved with the HNO_3 case.

Unlike NO_x , HNO_3 , and PAN, using the updated chemistry exacerbates an existing high-bias. The base case ozone predictions are high-biased throughout most of the

Title Page

Abstract

Introduction

Conclusions

References

Tables

Figures



Back

Close

Full Screen / Esc

Printer-friendly Version

Interactive Discussion



troposphere (excluding 1 to 3 km). The high-bias for ozone is likely the result of over-predictions of NO_y and NO_x . Figure 3a shows NO_y over-prediction from 0 to 8 km. The high-biased NO_y is well correlated with a high-bias seen for NO_x that extends throughout the same vertical structure.

The high-biased NO_x may be the result of lightning emissions that are highly uncertain. GEOS-Chem emits NO_x , produced from lightning flashes, according to a vertical profile published by Ott et al. (2010) shown in Fig. 2. The lightning profile shows a distinct similarity between normalized NO_x biases, as previously discussed. A high bias exists in the altitudes of 5 to 8 km, which corresponds to an area of high lightning flashes. The ratio of freshly emitted NO_x to HNO_3 shows a distinct similarity with the bi-modal lighting profiles observed by Ott et al. (2010) and recommend by Allen et al. (2011). Using a bi-modal distribution that would redistribute NO_x emissions from the middle troposphere to the upper and lower troposphere could improve the predictions. Overall, this update would improve the profile of NO_y and its component species, but would likely have to be accompanied by a downward revision to remove the NO_y high-bias.

When addressing the nitrogen partitioning in the lower troposphere, Fig. 3b shows that both models underpredict NO_x concentrations from 0 to 2 km. Though, once again, when normalized to NO_y , the HNO_3 case decreases the simulated low-bias. On a concentration basis, high bias exists for most species of NO_y . The HNO_3 case improves the predictions of HNO_3 but, significant improvements require the downward revision of NO_x , which is driving the over predictions of NO_y . For PAN in the lower atmosphere, Fig. 3d shows that both scenarios predict high speciation at the surface, as well. However, throughout the middle troposphere, the HNO_3 case increases the PAN normalized fraction.

Another important observation from Fig. 3 is that NO_y partitioning is altitude dependent. Near the surface, PAN is biased high ($[\text{PAN}]$ and $\text{PAN}:\text{NO}_y$) and NO_x is biased low as a fraction of NO_y . In the middle troposphere, NO_x is biased high (both $[\text{NO}_x]$ and

Chemical updates
and radiative effects

K. M. Seltzer et al.

Title Page

Abstract

Introduction

Conclusions

References

Tables

Figures



Back

Close

Full Screen / Esc

Printer-friendly Version

Interactive Discussion



$\text{NO}_x : \text{NO}_y$). In the middle and upper troposphere, HNO_3 concentration is biased high, but the $\text{HNO}_3 : \text{NO}_y$ is only biased high in the middle and upper troposphere.

3.2 Radiative effects evaluation

As previously mentioned, an offline radiative transfer model (PORT) was run, utilizing the output generated from the GEOS-Chem GCM. The input to this offline model included ozone, sulfate, organic and black hydrophilic and hydrophobic carbon, sea salt and dust. While many of these variables were not expected to be changed as a result of this mechanism update, each were included due to their availability. Each of these climate forcing variables were analyzed individually to determine the radiative effects associated with each climate variable. The complete difference associated with the mechanism update was also analyzed. As hypothesized, the results showed that ozone was the strongest contributor to surface and top of atmosphere direct radiative effects, with smaller and localized effects also observed for simulated differences in sulfate aerosols. These variables changes are due to the NO_x cycling that produces photochemical ozone and the changing atmospheric oxidation potential that the mechanism enables. The spatial and vertical changes, which further substantiate this assessment will be discussed further in the following section.

The PORT simulations had a spin-up period of 4-months to allow for radiative equilibrium due to the atmospheric perturbation. Following the spin-up period, the simulation was carried on for a full year to allow a calculation of a global annual average change in radiative forcing. In total, this method enabled a global annual average radiative effects determination that included all seasons; and the simulation time step allowed an even analysis of day and night forcings. As previously mentioned, the time step for this analysis was every 2190 min; which allowed a balance of computational strain and even season/daylight sampling routines. The global annual averaged change in radiative flux, including both solar and terrestrial radiation, at the surface from the updated nitric acid reaction rate was 6.8 mW m^{-2} . The global annual averaged change in radiation flux at the effective top of the atmosphere was 27.9 mW m^{-2} . The effective top of

Chemical updates and radiative effects

K. M. Seltzer et al.

Title Page

Abstract

Introduction

Conclusions

References

Tables

Figures



Back

Close

Full Screen / Esc

Printer-friendly Version

Interactive Discussion



**Chemical updates
and radiative effects**

K. M. Seltzer et al.

Title Page

Abstract

Introduction

Conclusions

References

Tables

Figures



Back

Close

Full Screen / Esc

Printer-friendly Version

Interactive Discussion



the atmosphere, in reality, is the top of the model, which is 2.194 hPa. As simulated, these values were driven strictly by the ozone and sulfate aerosol climate variables. Due to the increases in tropospheric ozone, the resulting change in radiative effects from ozone were a net positive gain. These increases were 31.1 mW m^{-2} at the top of the model and 10.4 mW m^{-2} at the surface. Similar to tropospheric ozone, there was a net increase in sulfate aerosols, which occurred mainly in the lower troposphere. This will be further discussed in the following section. However, in comparison to tropospheric ozone, this resulted in a net decrease in radiative effects. These decreases were -3.0 mW m^{-2} at the top of the model and -3.3 mW m^{-2} at the surface.

To put these global annual average values into perspective, the Intergovernmental Panel on Climate Change (IPCC) Assessment Report 5 (AR5) estimated that the total radiative forcing since pre-industrial times for ozone to be 350 mW m^{-2} . The values from these results cannot be directly applied to these IPCC values since the IPCC values are estimated to occur at the troposphere, as is the definition of radiative forcing. However, it can be assumed that the values from this study would result in a net flux change at the troposphere to be somewhere between the simulated surface and top of model values that were obtained. While the concentrations of tropospheric ozone have many determinants beyond the kinetic rate of nitric acid formation, the comparison of model predictions to published values of historical ozone forcing enables a comparative base line to analyze results against.

Figure 4 displays the annual averaged spatial distribution of radiative effects due to the changes in ozone from the updated mechanism. As seen, there is largely a net global increase in radiative forcing, which was hypothesized, due to the global increases of tropospheric ozone resulting from the mechanism update. In addition, it is observed that the maximum increases occur in the mid-latitude regions, with a slight decrease along the equator between the two mid-latitude regions. Also, a larger magnitude of forcing occurs at the top of atmosphere when compared to the surface. The net atmospheric forcing, which is the spatial plot at the bottom of the figure, is defined as the top of the atmosphere minus the surface forcing and has an influence on regional

**Chemical updates
and radiative effects**

K. M. Seltzer et al.

Title Page

Abstract

Introduction

Conclusions

References

Tables

Figures



Back

Close

Full Screen / Esc

Printer-friendly Version

Interactive Discussion



precipitation (Shindell et al., 2012). As seen in this portion of Fig. 4, the atmospheric forcing effects were entirely positive, with a maximum value situated near the equator. It is hypothesized that this result would cause precipitation increases in this portion of the world, which has the potential to further perturb the global radiation balance through indirect effects, which were not included in this simulation.

Figure 5 shows the radiative effects resulting from the changes in the atmospheric sulfate concentrations. These changes are a function of the localized adjustments in oxidative capacity due to the decrease in oxidation of NO_x . In contrast to Fig. 4 and the near global radiative effects associated with ozone, the simulated radiative changes associated with sulfate aerosols were only localized; and the local areas were only above landmasses, with the heaviest changes above highly polluted areas such as China and the Northeast United States. Also in contrast to the radiative effects associated with ozone, the radiative effects associated with the sulfate aerosols resulted in net decreases in the radiative flux. The longitudinally averaged portion of the plot shows near zero values at all latitudes due to the strongly localized nature of these changes. It is hypothesized that these localized, traditionally polluted areas, are limited in their capacity to oxidize SO_2 and the increase in hydroxyl radicals resulting from this mechanism update allowed the increase in production of sulfate aerosols.

3.3 Spatial assessment

This section describes the spatial concentration changes due to the revised chemistry kinetics. The analysis includes simulated changes to HNO_3 , NO_x , O_3 and SO_4 , on both horizontal and vertical patterns. As seen in Fig. 6, which displays the difference in HNO_3 and NO_x concentrations at the surface between the HNO_3 and Base Case simulations, the localized variations in both species had an obvious inverse relationship, and were nearly all localized over landmasses. However, the localized directional changes are counter intuitive to the assumed directional change that the mechanism update would create. These directional changes are strictly limited to the surface and quickly change throughout the troposphere, as shown in Fig. 7. Figure 7 shows that, once

again, the directional changes for HNO_3 and NO_x are inversely proportional throughout the troposphere, and the only areas of HNO_3 increase occur in the upper mid-latitudes at the surface. It should also be noted that stronger differences in HNO_3 and NO_x concentrations occurred in the upper troposphere, which was the targeted zone of evaluation for this project.

As shown in Fig. 8, the changes in the spatial distribution of ozone at the surface resulted in near global increases. A majority of the ozone changes occurred in the upper mid-latitudes and spanned the entire vertical atmosphere, as shown in Fig. 9. Vertically, most of the ozone changes occurred in the free troposphere, above the planetary boundary layer. The previous hypothesis that the changes in sulfate radiative effects were a result of changing oxidation potential were further review by looking at the spatial distribution of sulfate aerosol changes, as well. When reviewing Fig. 8, it is seen that the horizontal changes in sulfate at the surface occurred in the same localized regions as the surficial changes to HNO_3 and NO_x . When viewed on a vertical basis, Fig. 9 shows the the vertical changes to sulfate aerosol concentrations strictly occurred near the surface and did not follow the same trends as HNO_3 and NO_x , which had large differences throughout the troposphere.

4 Discussion

Literature updates to the $\text{NO}_2 + \text{HO}^\bullet$ reaction rate requires reanalysis of GEOS-Chem model performance and its sensitivity to the resulting chemistry. In this study, we have implemented updates to the GEOS-Chem chemistry and evaluated those updates during the INTEX-A observational campaign. Following an adjustment to this chemical mechanism, an evaluation of NO_y , its components and the resulting effects on atmospheric direct radiative effects were analyzed. We find that the base model has a high bias for NO_y , so NO_y components (NO_x , HNO_3 , and PAN) were evaluated as fractional components to determine how the mechanism effects speciation. Overall, the updated chemistry improves total oxidized nitrogen partitioning and decreases the termination

Chemical updates and radiative effects

K. M. Seltzer et al.

Title Page

Abstract

Introduction

Conclusions

References

Tables

Figures



Back

Close

Full Screen / Esc

Printer-friendly Version

Interactive Discussion



Chemical updates
and radiative effects

K. M. Seltzer et al.

Title Page

Abstract

Introduction

Conclusions

References

Tables

Figures



Back

Close

Full Screen / Esc

Printer-friendly Version

Interactive Discussion



of NO_x through the formation of nitric acid. In addition, since the oxidation of NO_x was decreases, a near global increase in ozone concentrations were seen. This increase resulted in changes to the oxidation potential of localized regions, which changes the concentration of resulting aerosol formation. All of these results have a relationship with the simulated radiation budget of the atmosphere.

The updated $\text{NO}_2 + \text{HO}^\bullet$ chemistry improves simulated partitioning of NO_x , PAN, and HNO_3 throughout most of the atmosphere. In the upper troposphere, where this analysis was mainly targeting improved simulation results, the updated chemical mechanism improves modeled results for all NO_y components above 8 km. In the middle troposphere, HNO_3 and PAN also experience improvements in predictions; however, the updated chemistry exacerbates a base model bias for NO_x that may be caused by the lightning emission profile.

While the updated chemistry helped improve the predictions of speciated NO_y at most levels of the atmosphere, several model biases are still observed. This includes over predictions of NO_x and NO_y in the middle troposphere and underpredictions for PAN at most altitudes. As mentioned previously, it is hypothesized that NO_x , and in turn NO_y , would be improved with an update to the lightning emission profile. The performance of PAN is most likely tied to the low-bias for acetaldehyde and $\text{HO}_2^\bullet : \text{HO}^\bullet$. The low-bias in $\text{HO}_2^\bullet : \text{HO}^\bullet$ is caused by a high-bias for HO^\bullet . The high-biased HO^\bullet would preferentially remove fast reacting compounds like acetaldehyde ($k_{\text{HO}^\bullet} = 4.63 \times 10^{-12} \times \exp(350/T)$) compared to acetaldehyde's precursors, ethane ($k_{\text{HO}^\bullet} = 7.6 \times 10^{-12} \times \exp(-1020/T)$) and ethanol ($k_{\text{HO}^\bullet} = 3.15 \times 10^{-14}$). This suggests, as did Millet et al. (2010), that there is not, in fact, a missing source of acetaldehyde. Instead, an imbalance caused by over-predicted sinks causes acetaldehyde underpredictions that lead to low $\text{CH}_3\text{C}(\text{O})\text{OO}^\bullet$ radicals and reduced PAN formation. The updated chemistry used here exacerbates the HO^\bullet bias, and more research is necessary to constrain this problem.

Like the improvements in oxidized nitrogen, the change in simulated ozone sensitivity is modest. The updated model uses NO_x more efficiently and, therefore, is more

**Chemical updates
and radiative effects**

K. M. Seltzer et al.

Title Page

Abstract

Introduction

Conclusions

References

Tables

Figures



Back

Close

Full Screen / Esc

Printer-friendly Version

Interactive Discussion



responsive to incremental reductions of NO_x . In response to reduced NO_x emissions, the sensitivity of predicted O_3 concentrations was never more than a couple percent different based on updated chemistry. At the surface, where air quality is the primary concern, the updated chemistry increases sensitivity the least and the largest changes are seen at the mid-latitudes in the middle to upper troposphere. The larger differences in the upper troposphere are most likely due to long-range transport. As a result to these changes in tropospheric ozone, simulated climate forcing due to this climate variable were evaluated.

The changing atmospheric chemistry, mainly relating to ozone and sulfate aerosols, experienced changes due to this mechanism update. By utilizing an offline radiative transfer model, the radiative effects resulting from this kinetic update were quantified. Radiative effects were seen in both the solar and terrestrial forms of the radiation spectrum, and were mainly caused by differences in ozone, with slight effects from sulfate aerosols. Overall, a positive net flux of 6.8 mW m^{-2} and a positive net flux of 27.9 mW m^{-2} was quantified for the surface and the top of the atmosphere, respectively. Ozone contributed radiative effects in both the solar and terrestrial forms of radiative energy while sulfate only contributed effects in the solar form through scattering processes. The radiative effects from ozone were seen globally, with maximum variances seen in the mid-latitudes. In contrast, the radiative effects resulting from the changes in sulfate concentrations were limited to areas over landmasses, and has the strongest influences over China and the Northeast United States. Overall, a positive net flux of 10.4 mW m^{-2} and a negative net flux of 3.3 mW m^{-2} was quantified for the surface for ozone and sulfate aerosols, respectively.

This study demonstrates that updates to the chemical mechanism improves precursor performance without drastically changing the policy implications of the model. The sensitivity of the model, as evaluated in this paper, however, is relative to a model that is high-biased for NO_y concentrations. Improvements to the global emission inventories could alter the relative sensitivities in this study, but conclusions were robust when used with two versions of the NEI (NEI99 not shown). The chemistry updates for the

rate of $\text{NO}_2 + \text{HO}^\bullet$ used in this study also need confirmation by more laboratory and field studies. The rate of $\text{NO}_2 + \text{HO}^\bullet$ is key to the inorganic and organic chemical cycling that drives ozone production, and acceptance of updates to this rate will require a preponderance of evidence.

5 Appendix A: Total oxidized nitrogen concentrations

The main text shows total oxidized nitrogen partitioning (see Fig. 3), but not concentrations of component species NO_y , NO_x , HNO_3 , or PAN. Figure A1 provides concentration data to complement Fig. 3.

10 *Acknowledgements.* Special thanks Rob Pinder, Farhan Akhtar and to Melody Avery, Donald Blake, William Brune, Alan Fried, Brian Heikes, Greg Huey, Glen Sachse, Hanwant Singh, and the INTEX team for the DC8 observational data.

References

- 15 Allen, D. J., Pickering, K. E., Pinder, R. W., Henderson, B. H., Appel, K. W., and Prados, A.: Impact of lightning-NO on eastern United States photochemistry during the summer of 2006 as determined using the CMAQ model, *Atmos. Chem. Phys.*, 12, 1737–1758, doi:10.5194/acp-12-1737-2012, 2012. 3233
- Atkinson, R., Baulch, D. L., Cox, R. A., Crowley, J. N., Hampson, R. F., Hynes, R. G., Jenkin, M. E., Rossi, M. J., and Troe, J.: Evaluated kinetic and photochemical data for atmospheric chemistry: Volume I – gas phase reactions of O_x , HO_x , NO_x and SO_x species, *Atmos. Chem. Phys.*, 4, 1461–1738, doi:10.5194/acp-4-1461-2004, 2004. 3224
- 20 Bertram, T. H., Perrring, A. E., Wooldridge, P. J., Crounse, J. D., Kwan, A. J., Wennberg, P. O., Scheuer, E., Dibb, J., Avery, M., Sachse, G., Vay, S. A., Crawford, J. H., McNaughton, C. S., Clarke, A., Pickering, K. E., Fuelberg, H., Huey, G., Blake, D. R., Singh, H. B., Hall, S. R., Shetter, R. E., Fried, A., Heikes, B. G., and Cohen, R. C.: Direct measurements of the convective recycling of the upper troposphere, *Science*, 315, 816–820, doi:10.1126/science.1134548, 2007. 3226
- 25

Chemical updates
and radiative effects

K. M. Seltzer et al.

Title Page

Abstract

Introduction

Conclusions

References

Tables

Figures



Back

Close

Full Screen / Esc

Printer-friendly Version

Interactive Discussion



- Browne, E. C., Perring, A. E., Wooldridge, P. J., Apel, E., Hall, S. R., Huey, L. G., Mao, J., Spencer, K. M., Clair, J. M. St., Weinheimer, A. J., Wisthaler, A., and Cohen, R. C.: Global and regional effects of the photochemistry of $\text{CH}_3\text{O}_2\text{NO}_2$: evidence from ARCTAS, *Atmos. Chem. Phys.*, 11, 4209–4219, doi:10.5194/acp-11-4209-2011, 2011. 3225
- 5 Chameides, W. L., Fehsenfeld, F., Rodgers, M. O., Cardelino, C., Martinez, J., Parrish, D., Lonnenman, W., Lawson, D. R., Rasmussen, R. A., Zimmerman, P., Greenberg, J., Middleton, P., and Wang, T.: Ozone precursor relationships in the ambient atmosphere, *J. Geophys. Res.*, 97, 6037, doi:10.1029/91JD03014, 1992. 3221
- Chen, D., Wang, Y., McElroy, M. B., He, K., Yantosca, R. M., and Le Sager, P.: Regional CO pollution and export in China simulated by the high-resolution nested-grid GEOS-Chem model, *Atmos. Chem. Phys.*, 9, 3825–3839, doi:10.5194/acp-9-3825-2009, 2009. 3220
- 10 Cohan, D. S., Koo, B., and Yarwood, G.: Influence of uncertain reaction rates on ozone sensitivity to emissions, *Atmos. Environ.*, 44, 3101–3109, doi:10.1016/j.atmosenv.2010.05.034, 2010. 3222
- 15 Conley, A. J., Lamarque, J.-F., Vitt, F., Collins, W. D., and Kiehl, J.: PORT, a CESM tool for the diagnosis of radiative forcing, *Geosci. Model Dev.*, 6, 469–476, doi:10.5194/gmd-6-469-2013, 2013. 3231
- Dallmann, T. R. and Harley, R. A.: Evaluation of mobile source emission trends in the United States, *J. Geophys. Res.*, 115, D14305, doi:10.1029/2010JD013862, 2010. 3223
- 20 Donahue, N. M.: Atmospheric chemistry: the reaction that wouldn't quit, *Nature Chemistry*, 3, 98–99, doi:10.1038/nchem.941, 2011. 3221, 3224
- Fusco, A. C. and Logan, J.: Analysis of 1970–1995 trends in tropospheric ozone at Northern Hemisphere midlatitudes with the GEOS-CHEM model, *J. Geophys. Res.*, 108(D15), 4449, doi:10.1029/2002JD002742, 2003. 3220
- 25 Guenther, A., Karl, T., Harley, P., Wiedinmyer, C., Palmer, P. I., and Geron, C.: Estimates of global terrestrial isoprene emissions using MEGAN (Model of Emissions of Gases and Aerosols from Nature), *Atmos. Chem. Phys.*, 6, 3181–3210, doi:10.5194/acp-6-3181-2006, 2006. 3223
- Henderson, B. H., Pinder, R. W., Crooks, J., Cohen, R. C., Carlton, A. G., Pye, H. O. T., and Vizuete, W.: Combining Bayesian methods and aircraft observations to constrain the $\text{HO}^\bullet + \text{NO}_2$ reaction rate, *Atmos. Chem. Phys.*, 12, 653–667, doi:10.5194/acp-12-653-2012, 2012. 3221, 3224, 3225

Chemical updates
and radiative effects

K. M. Seltzer et al.

Title Page

Abstract

Introduction

Conclusions

References

Tables

Figures



Back

Close

Full Screen / Esc

Printer-friendly Version

Interactive Discussion



- Hudman, R. C., Jacob, D. J., Turquety, S., Leibensperger, E. M., Murray, L. T., Wu, S., Gilliland, A. B., Avery, M., Bertram, T. H., Brune, W., Cohen, R. C., Dibb, J. E., Flocke, F. M., Fried, A., Holloway, J., Neuman, J. A., Orville, R., Perring, A., Ren, X., Sachse, G. W., Singh, H. B., Swanson, A., and Wooldridge, P. J.: Surface and lightning sources of nitrogen oxides over the United States: Magnitudes, chemical evolution, and outflow, *J. Geophys. Res.*, 112, D12S05, doi:10.1029/2006JD007912, 2007. 3224
- Jacob, D. J., Logan, J. A., Gardner, G. M., Yevich, R. M., Spivakovsky, C. M., Wofsy, S. C., Sillman, S., and Prather, M. J.: Factors regulating ozone over the United States and its export to the global atmosphere, *J. Geophys. Res.*, 98, 14817, doi:10.1029/98JD01224, 1993. 3221
- Jaeglé, L., Jacob, D. J., Brune, W. H., Tan, D., Faloon, I. C., Weinheimer, A. J., Ridley, B. A., Campos, T. L., and Sachse, G. W.: Sources of HO_x and production of ozone in the upper troposphere over the United States, *Geophys. Res. Lett.*, 25, 1709–1712, doi:10.1029/98GL00041, 1998. 3221
- Jaeglé, L., Jaffe, D., Price, H., Weiss-Penzias, P., Palmer, P., Evans, M., Jacob, D., and Bey, I.: Sources and budgets for CO and O₃ in the northeastern Pacific during the spring of 2001: Results from the PHOBEA-II Experiment, *J. Geophys. Res.*, 108(D20), 8802, doi:10.1029/2002JD003121, 2003. 3220
- Kopacz, M., Jacob, D. J., Fisher, J. A., Logan, J. A., Zhang, L., Megretskaia, I. A., Yantosca, R. M., Singh, K., Henze, D. K., Burrows, J. P., Buchwitz, M., Khlystova, I., McMillan, W. W., Gille, J. C., Edwards, D. P., Eldering, A., Thouret, V., and Nedelec, P.: Global estimates of CO sources with high resolution by adjoint inversion of multiple satellite datasets (MOPITT, AIRS, SCIAMACHY, TES), *Atmos. Chem. Phys.*, 10, 855–876, doi:10.5194/acp-10-855-2010, 2010. 3220
- Kuhns, H., Green, M., and Etyemezian, V.: Big Bend Regional Aerosol and Visibility Observational (BRAVO) Study Emissions Inventory, Desert Research Institute, 2003. 3223
- McKeen, S. A., Hsie, E.-Y., and Liu, S. C.: A study of the dependence of rural ozone on ozone precursors in the eastern United States, *J. Geophys. Res.*, 96, 15377, doi:10.1029/91JD01282, 1991. 3221
- Millet, D. B., Guenther, A., Siegel, D. A., Nelson, N. B., Singh, H. B., de Gouw, J. A., Warneke, C., Williams, J., Eerdekens, G., Sinha, V., Karl, T., Flocke, F., Apel, E., Riemer, D. D., Palmer, P. I., and Barkley, M.: Global atmospheric budget of acetaldehyde: 3-D model analysis and constraints from in-situ and satellite observations, *Atmos. Chem. Phys.*, 10, 3405–3425, doi:10.5194/acp-10-3405-2010, 2010. 3220, 3238

**Chemical updates
and radiative effects**

K. M. Seltzer et al.

Title Page

Abstract

Introduction

Conclusions

References

Tables

Figures



Back

Close

Full Screen / Esc

Printer-friendly Version

Interactive Discussion



- Mollner, A. K., Valluvadasan, S., Feng, L., Sprague, M. K., Okumura, M., Milligan, D. B., Bloss, W. J., Sander, S. P., Martien, P. T., Harley, R. A., McCoy, A. B., and Carter, W. P. L.: Rate of gas phase association of hydroxyl radical and nitrogen dioxide, *Science*, 330, 646–649, doi:10.1126/science.1193030, 2010. 3221, 3224
- 5 Olivier, J., Berdowski, J., Peters, J., Bakker, J., Visschedijk, A., and Bloos, J.: Applications of EDGAR emission database for global Atmospheric Research, RIVM report 773301001/NRP report 410 200 051, 2002. 3224
- Ott, L. E., Pickering, K. E., Stenchikov, G. L., Allen, D. J., DeCaria, A. J., Ridley, B., Lin, R.-F., Lang, S., and Tao, W.-K.: Production of lightning NO_x and its vertical distribution calculated from three-dimensional cloud-scale chemical transport model simulations, *J. Geophys. Res.*, 115, D04301, doi:10.1029/2009JD011880, 2010. 3223, 3233
- 10 Parrish, D. D.: Critical evaluation of US on-road vehicle emission inventories, *Atmos. Environ.*, 40, 2288–2300, doi:10.1016/j.atmosenv.2005.11.033, 2006. 3223
- Sander, S., Abbatt, J., Barker, J., Burkholder, J., Friedl, R., Golden, D., Huie, R., Kolb, C., Kurylo, M., Moortgat, G., Orkin, V., and Wine, P.: Chemical Kinetics and Photochemical Data for Use in Atmospheric Studies, Evaluation No. 17, JPL Publication 10-6, Jet Propulsion Laboratory, Pasadena, available at: <http://jpldataeval.jpl.nasa.gov>, 2011. 3224
- 15 Schuirmann, D. J.: A comparison of the two one-sided tests procedure and the power approach for assessing the equivalence of average bioavailability, *J. Pharmacokinet. Biop.*, 15, 657–680, doi:10.1007/BF01068419, 1987. 3228
- Seinfeld, J. H.: Urban air pollution: state of the science, *Science*, 243, 745–752, doi:10.1126/science.243.4892.745, 1989. 3221
- Shindell, D., Kuylenstierna, J. C. I., Vignati, E., van Dingenen, R., Amann, M., Klimont, Z., Anenberg, S. C., Muller, N., Janssens-Maenhout, G., Raes, F., Schwartz, J., Faluvegi, G., Pozzoli, L., Kupiainen, K., Hoglund-Isaksson, L., Emberson, L., Streets, D., Ramanathan, V., Hicks, K., Oanh, N. T. K., Milly, G., Williams, M., Demkine, V., and Fowler, D.: Simultaneously mitigating near-term climate change and improving human health and food security, *Science*, 335, 183–189, doi:10.1126/science.1210026, 2012. 3236
- 25 Sillman, S., Logan, J. A., and Wofsy, S. C.: The sensitivity of ozone to nitrogen oxides and hydrocarbons in regional ozone episodes, *J. Geophys. Res.*, 95, 1837, doi:10.1029/JD095iD02p01837, 1990. 3221
- 30 Singh, H. B., Salas, L., Herlth, D., Kolyer, R., Czech, E., Avery, M., Crawford, J. H., Pierce, R. B., Sachse, G. W., Blake, D. R., Cohen, R. C., Bertram, T. H., Perring, A., Wooldridge, P. J.,

Chemical updates
and radiative effects

K. M. Seltzer et al.

Title Page

Abstract

Introduction

Conclusions

References

Tables

Figures



Back

Close

Full Screen / Esc

Printer-friendly Version

Interactive Discussion



Dibb, J., Huey, G., Hudman, R. C., Turquety, S., Emmons, L. K., Flocke, F., Tang, Y., Carmichael, G. R., and Horowitz, L. W.: Reactive nitrogen distribution and partitioning in the North American troposphere and lowermost stratosphere, *J. Geophys. Res.*, 112, D12S04, doi:10.1029/2006JD007664, 2007. 3226

5 Streets, D. G., Bond, T., Carmichael, G. R., Fernandes, S., Fu, Q., He, D., Kilmont, Z., Nelson, S., Tsai, N., Wang, M., Woo, J., and Yarber, K.: An inventory of gaseous and primary aerosol emissions in Asia in the year 2000, *J. Geophys. Res.*, 108(D21), 8809, doi:10.1029/2002JD003093, 2003. 3224

10 Streets, D. G., Zhang, Q., Wang, L., He, K., Hao, J., Wu, Y., Tang, Y., and Carmichael, G. R.: Revisiting China's CO emissions after the Transport and Chemical Evolution over the Pacific (TRACE-P) mission: synthesis of inventories, atmospheric modeling, and observations, *J. Geophys. Res.*, 111, D14306, doi:10.1029/2006JD007118, 2006. 3224

15 van der Werf, G. R., Randerson, J. T., Giglio, L., Collatz, G. J., Kasibhatla, P. S., and Arelano Jr., A. F.: Interannual variability in global biomass burning emissions from 1997 to 2004, *Atmos. Chem. Phys.*, 6, 3423–3441, doi:10.5194/acp-6-3423-2006, 2006. 3223

Vestreng, V. and Klein, H.: Emission data reported to UNECE/EMEP: Quality assurance and trend analysis & Presentation of WebDab, MSC-W Status Rep. 2002, 2002. 3223

Welch, B. L.: The Generalization of “Student's” problem when several different population variances are involved, *Biometrika*, 34, 28–35, doi:10.1093/biomet/34.1-2.28, 1947. 3227

20 West, J. J., Fiore, A. M., Horowitz, L. W., and Mauzerall, D. L.: Global health benefits of mitigating ozone pollution with methane emission controls, *P. Natl. Acad. Sci. USA*, 103, 3988–3993, doi:10.1073/pnas.0600201103, 2006. 3220

25 West, J. J., Naik, V., Horowitz, L. W., and Fiore, A. M.: Effect of regional precursor emission controls on long-range ozone transport – Part 2: Steady-state changes in ozone air quality and impacts on human mortality, *Atmos. Chem. Phys.*, 9, 6095–6107, doi:10.5194/acp-9-6095-2009, 2009. 3220

Chemical updates
and radiative effects

K. M. Seltzer et al.

Title Page

Abstract

Introduction

Conclusions

References

Tables

Figures

◀

▶

◀

▶

Back

Close

Full Screen / Esc

Printer-friendly Version

Interactive Discussion



Table 1. Measurement descriptive statistics (mean: \bar{X} , percentiles: 5, 50, 90 %), average relative uncertainty as a percent ($\frac{\sigma_x}{\bar{X}}$ %), and absolute uncertainty in measurement units.

Measured (unit)	N	\bar{X}	5 %	50 %	95 %	$\frac{\sigma_x}{\bar{X}}$ %	$\bar{\sigma}$
Lat (deg)	4015	40.0	29.1	40.2	49.7	N/A	N/A
Long (deg)	4015	281.3	257.4	280.7	304.7	N/A	N/A
Alt (km)	4015	4.9	0.3	4.6	10.1	N/A	N/A
HO ₂	3803	21.3	8.1	18.7	41.5	15.0	3.2
OH (1×10^{-3} ppt)	3904	348.8	102.4	300.4	778.6	15.0	52.3
NO	3745	95.1	4.9	30.1	361.9	7.3	6.9
NO ₂	3995	94.9	7.8	39.8	335.4	5.0	4.7
HNO ₄	2399	37.5	1.5	24.2	111.4	23.0	8.6
PAN	3046	268.9	13.0	225.8	658.4	15.0	40.3
HNO ₃	2423	420.6	59.8	313.2	1109.8	21.0	51.1
NO _x	3745	182.1	14.3	77.4	621.7	4.7	9.0
NO _z = PAN + HNO ₃	1818	680.2	165.7	569.6	1527.8	12.2	68.3
NO _y = NO _x + PAN + HNO ₃	1743	819.0	208.4	668.4	1919.1	9.9	68.3
O ₃ (ppb)	4015	61.9	32.8	60.6	92.4	5.0	3.1
H ₂ O ₂	2435	1263.7	122.8	976.9	3209.5	13.5	173.2
CO (ppm)	4015	104.5	71.5	102.9	141.4	2.0	2.1
CH ₂ O	2856	717.6	47.0	394.0	2518.5	50.6	118.8
CH ₃ CHO	1837	130.3	10.0	103.6	343.2	20.0	26.1
CH ₃ C(O)CH ₃	1827	1766.8	663.1	1525.9	3669.9	20.0	353.4

Chemical updates and radiative effects

K. M. Seltzer et al.

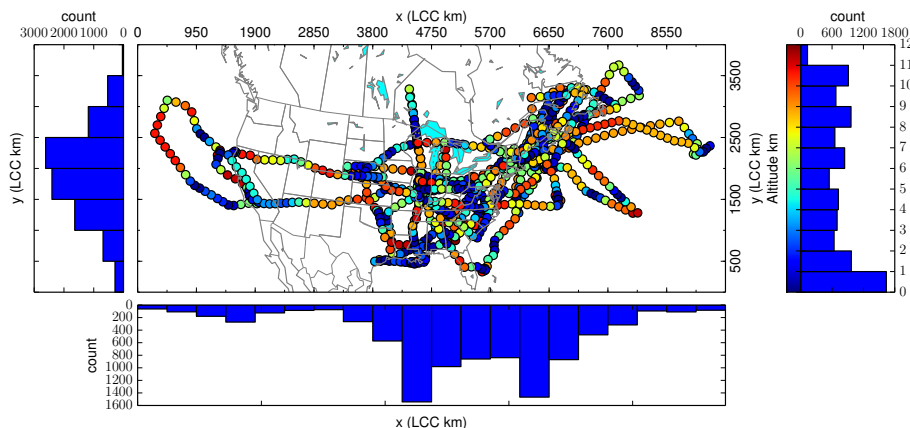


Figure 1. Sample locations (dots) from the INTEX-A campaign with altitude shown in color with histograms for latitude and longitude. The dots show every tenth sample, but the histograms use all samples.

Title Page

Abstract

Introduction

Conclusions

References

Tables

Figures

◀

▶

◀

▶

Back

Close

Full Screen / Esc

Printer-friendly Version

Interactive Discussion



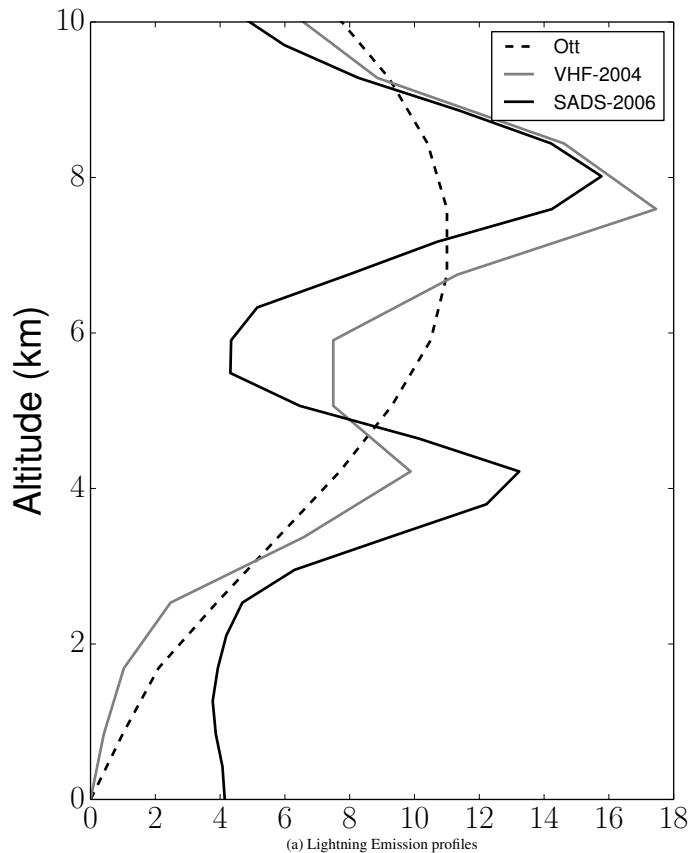


Figure 2. Lightning emission profiles (VHF-2004 and SADS-2006).

Chemical updates and radiative effects

K. M. Seltzer et al.

Title Page

Abstract Introduction

Conclusions References

Tables Figures

◀ ▶

◀ ▶

Back Close

Full Screen / Esc

Printer-friendly Version

Interactive Discussion



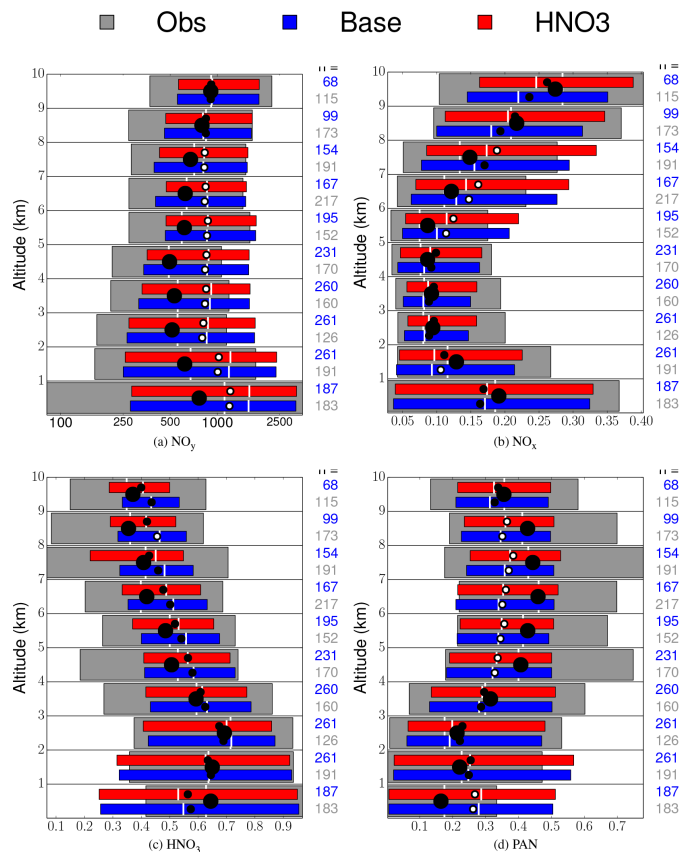


Figure 3. Model evaluation at 10 1 km altitude bins. Each panel shows 5th to 95th percentile range (box), median (white line), and mean (circle) for observations (grey), the base case (blue), and the HNO₃ case (red). When the circle is filled in, the predictions cannot be rejected as within the uncertainty range. Number of observations (black) and model points (blue) per 1 km bin are detailed in the margin.

Chemical updates
and radiative effects

K. M. Seltzer et al.

Title Page

Abstract

Introduction

Conclusions

References

Tables

Figures



Back

Close

Full Screen / Esc

Printer-friendly Version

Interactive Discussion

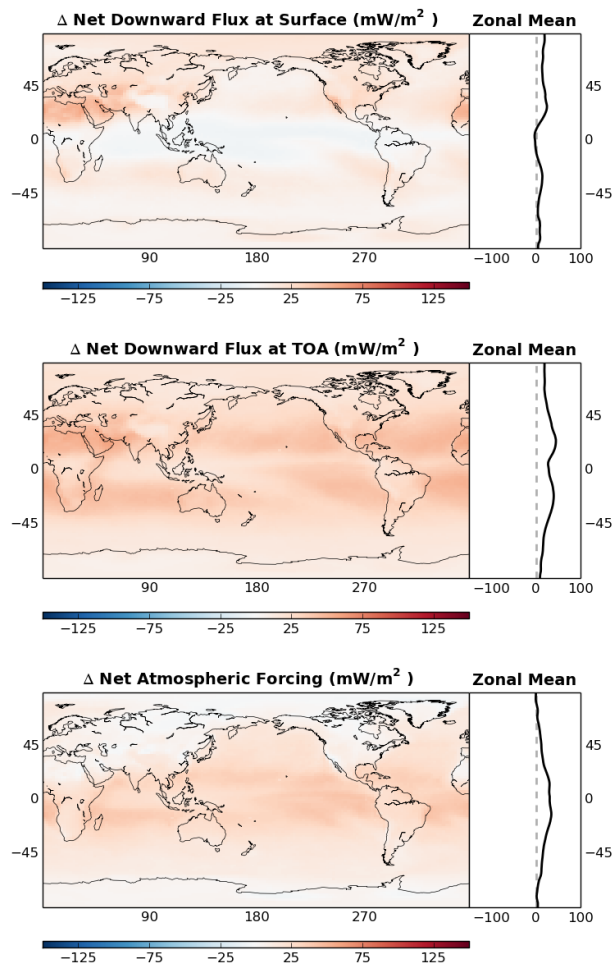


Figure 4. Net downward flux, in mWm^{-2} , at the surface (top) and top of model (middle) for ozone. Net downward atmospheric forcing shown in bottom plot for ozone.

Chemical updates
and radiative effects

K. M. Seltzer et al.

Title Page

Abstract

Introduction

Conclusions

References

Tables

Figures



Back

Close

Full Screen / Esc

Printer-friendly Version

Interactive Discussion

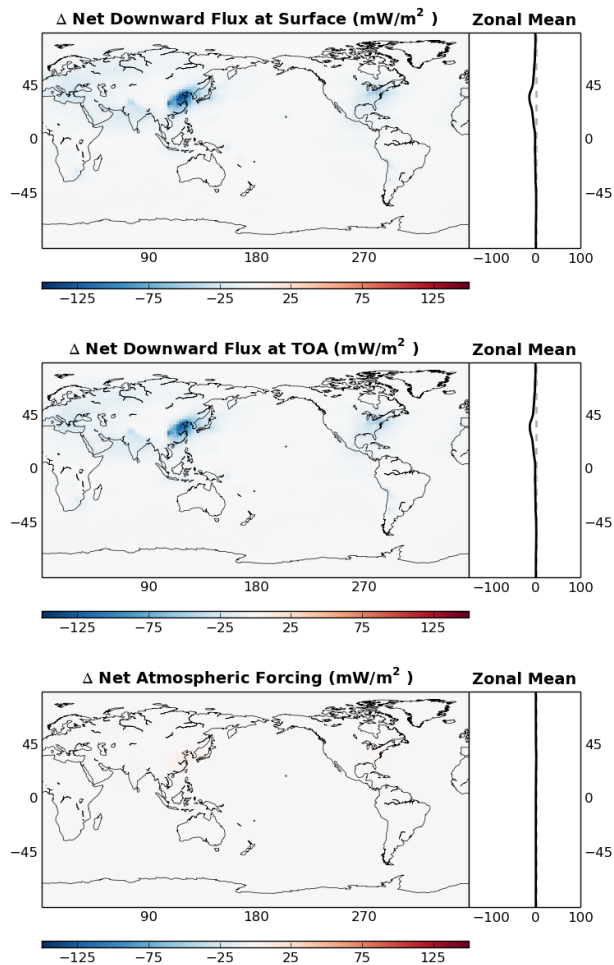


Figure 5. Net downward flux, in mW m^{-2} , at the surface (top) and top of model (middle) for sulfate aerosols. Net downward atmospheric forcing shown in bottom plot for sulfate aerosols.

Chemical updates
and radiative effects

K. M. Seltzer et al.

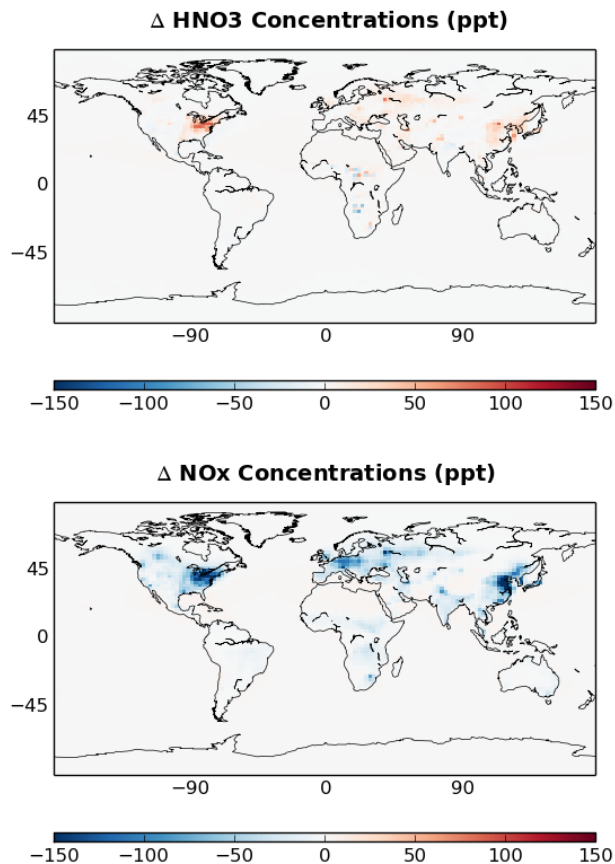


Figure 6. Difference in mean HNO₃ and NO_x mixing ratios between the HNO₃ and base case simulations for the surface layer.

[Title Page](#)[Abstract](#)[Introduction](#)[Conclusions](#)[References](#)[Tables](#)[Figures](#)[◀](#)[▶](#)[◀](#)[▶](#)[Back](#)[Close](#)[Full Screen / Esc](#)[Printer-friendly Version](#)[Interactive Discussion](#)

Chemical updates
and radiative effects

K. M. Seltzer et al.

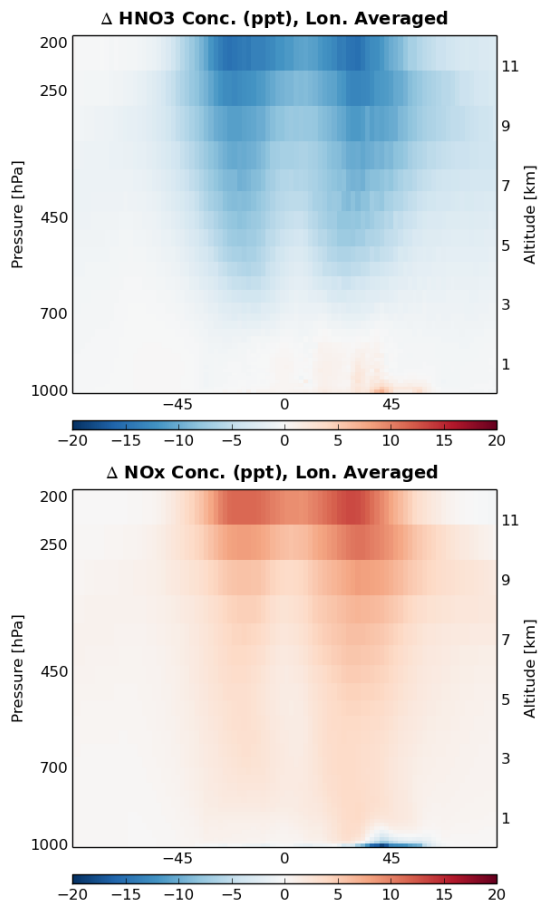


Figure 7. Vertical difference in mean HNO₃ and NO_x mixing ratios between the HNO₃ and base case simulations (longitudinally averaged values).

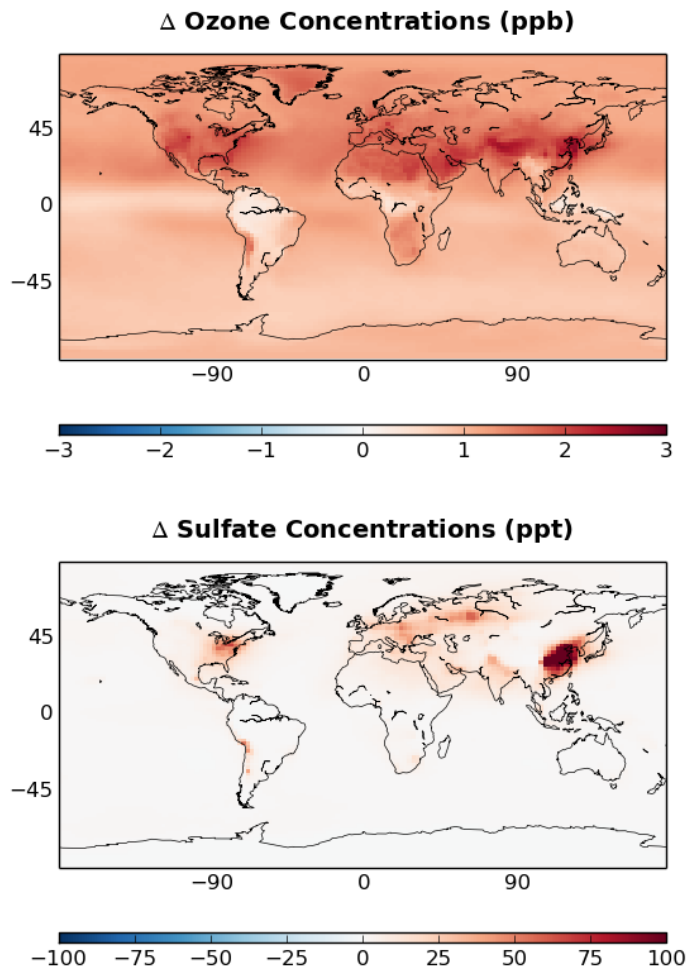


Figure 8. Difference in mean O₃ and sulfate mixing ratios between the HNO₃ and base case simulations for the surface layer.

Title Page

Abstract

Introduction

Conclusions

References

Tables

Figures

◀

▶

◀

▶

Back

Close

Full Screen / Esc

Printer-friendly Version

Interactive Discussion



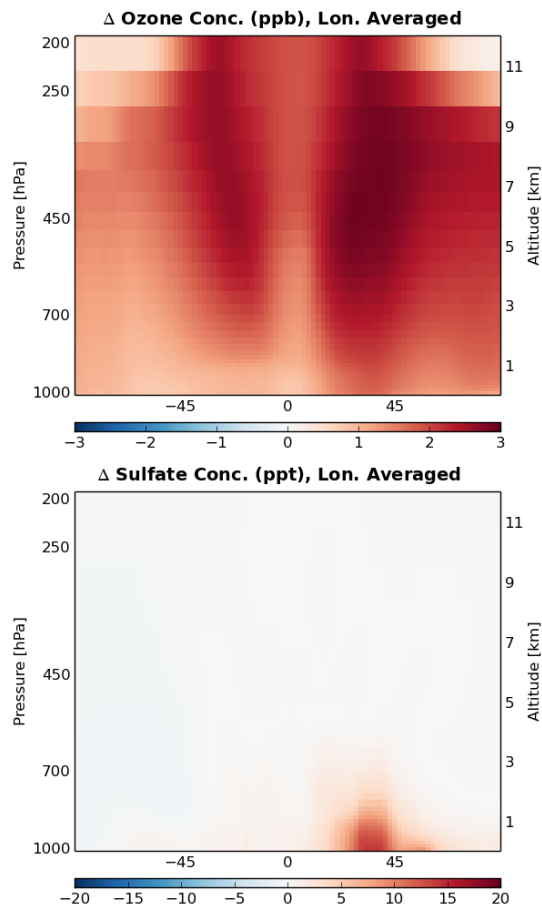


Figure 9. Vertical difference in mean O₃ and sulfate mixing ratios between the HNO₃ and base case simulations (longitudinally averaged values).

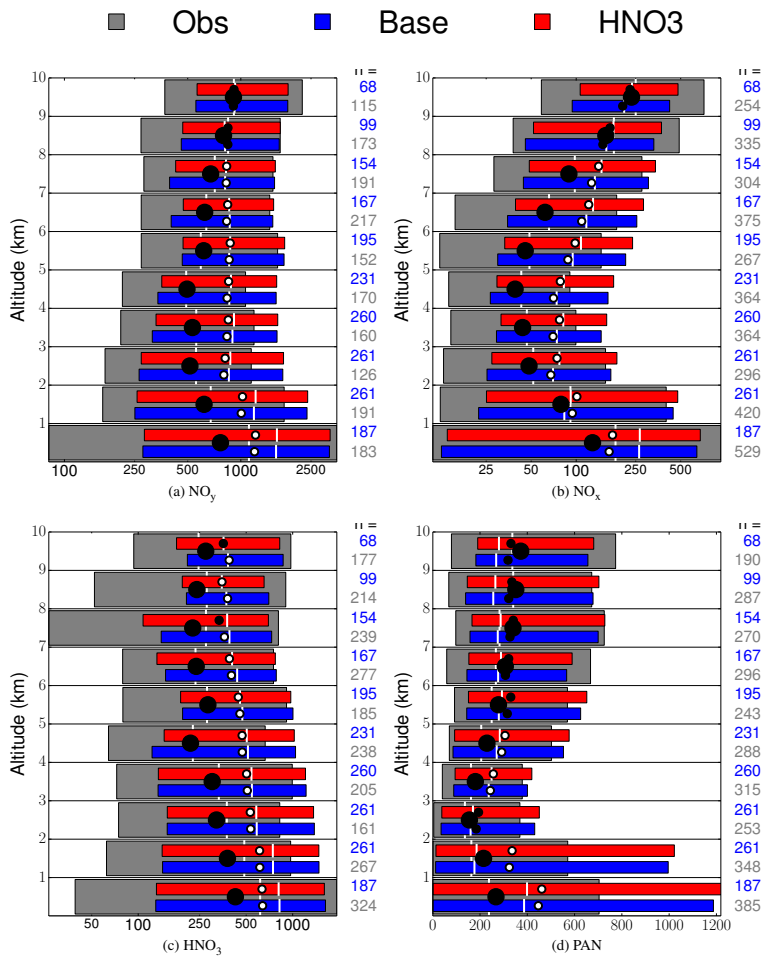


Figure A1. Same as Fig. 3 for concentrations instead of NO_y fractions.

Title Page

Abstract

Introduction

Conclusions

References

Tables

Figures



Back

Close

Full Screen / Esc

Printer-friendly Version

Interactive Discussion

